# Resting multivoxel activity patterns in human visual cortex are linked to patterns evoked by preferred visual stimuli

Name: DoHyun Kim[1], Tomer Livne[2], Nicholas V. Metcalf[3], Maurizio Corbetta[3,4,5,6], Gordon L. Shulman[3]

Departments of [1]Biomedical Engineering, [3]Neurology, [4]Radiology, and [5]Anatomy & Neurobiology at Washington University School of Medicine, St. Louis, MO, USA

Department of [2]Neurobiology, Weizmann Institution of Science, Israel.

Department of [6]Neurology, University of Padua, Italy

Correspondence: Gordon L. Shulman

E-mail: gshulman@wustl.edu

**Keywords**: BOLD, fMRI, Intrinsic activity, multivariate pattern analysis (MVPA), Resting-state.

## Abstract

The relationship between spontaneous and task-evoked brain activity is an increasingly important topic in neuroscience. Here, we ask if spontaneous multivoxel activity patterns in human visual cortex are linked to patterns evoked by naturalistic (e.g. faces) and non-naturalistic (e.g. phase-scrambled faces) visual stimuli. We identified regions that preferred particular stimulus categories during localizer scans, combined those regions into joint-ROIs, and measured multivoxel patterns in the joint-ROIs for each stimulus class during task scans. We then spatially correlated these stimulus-evoked patterns to the multivoxel pattern measured in each frame of resting-state scans. The mean correlation coefficient was essentially zero for all regions/stimulus categories, indicating that resting activity patterns were not biased toward particular stimuli. However, the spread of correlation coefficients (positive, negative) was significantly greater for a joint-ROI's preferred stimulus. Moreover, at single timepoints the resting multivoxel patterns in constituent ROIs of a joint-ROI were not independent but formed a coherent brain state. Therefore, spontaneous activity patterns were coherent across regions, and maximally varied within a region in the degree to which they positively or negatively matched the pattern evoked by the region's preferred stimulus. We conclude that in human visual cortex spontaneous multi-voxel activity patterns are linked to stimulus-evoked patterns.

## Introduction

The functional role of spontaneous brain activity in human behavior is an increasingly important topic in neuroscience. An emerging view is that the neural activity evoked by a task and the associated behavior is influenced and constrained by ongoing neural activity (Tsodyks et al. 1999; Fiser et al. 2004; Fox et al. 2007; Cole et al. 2016; Tavor et al. 2016) an idea that contrasts with a long-standing view that spontaneous activity is random, and only important as a mechanism for facilitating forward transmission of information processing (Shadlen and Newsome 1994). Many studies have now shown that spontaneous activity is highly structured in space and time (Biswal et al. 1995; Greicius et al. 2003; Kenet et al. 2003; He et al. 2008; de Pasquale et al. 2010; Power et al. 2011; Yeo et al. 2011). Imaging of neural activity at a scale that extends across many cortical columns has shown that the macro-scale pattern of spontaneous neural activity within a sensory area in an anesthetized animal mirrors the pattern of activity evoked by stimulation of a specific visual feature (Kenet et al. 2003; Omer et al. 2018). Moreover, stimulus-evoked activity can be predicted from the ongoing activity that occurs before or coincident with stimulus onset (Arieli et al. 1996; Tsodyks et al. 1999).

On a more global scale, human imaging studies have shown that widely distributed regions that are co-activated during a task show temporally correlated activity at rest(Biswal et al. 1995; Fox et al. 2005; Smith et al. 2009). For example, human frontal eye field (FEF) and dorsal intraparietal sulcus (IPS) or superior parietal lobule (SPL) are routinely co-activated in tasks that involve oculomotor or visuospatial attentional demands and also show highly correlated activity at rest(Fox et al. 2006). In

fact, the blood-oxygenation-level-dependent (BOLD) activity in large groups of regions at rest are highly correlated, forming what are termed resting-state networks (RSNs) that are associated with particular functions (e.g. dorsal attention network) (Power et al. 2011; Yeo et al. 2011). The measurement of interregional correlations at rest, functional connectivity magnetic resonance imaging (fcMRI), has become a primary tool for measuring spontaneous interactions between brain regions. Moreover, a growing body of work is using fcMRI to understand and assess brain damage and disease (He et al. 2007; Sheline and Raichle 2013; Sharp et al. 2014; Gao and Wu 2016).

The relationship between resting and task-evoked activity in fMRI studies has been conceptualized in terms of the correspondence between resting and task networks defined by inter-regional correlations (Cole et al. 2014; Kim et al. 2018), or between resting networks and patterns of task co-activation(Smith et al. 2009). Also, recent studies have examined whether task activation can be predicted from resting functional connectivity (FC) (Cole et al. 2016; Tavor et al. 2016). Here, we discuss a conceptualization more related to the animal work noted above, which provides novel insight into why rest-task correspondences occur and thus, the function of spontaneous activity. This conceptualization posits that statistical regularities in the external and internal (motor planning, cognitive routines) environment result in similar distributions of the neural states encoding those regularities (Fiser et al. 2010). Resting states in turn reflect these high-information neural states through a Hebbian learning process (Lewis et al. 2009). Studies have shown that performing a task changes FC in subsequent resting epochs (Albert et al. 2009; Hasson et al. 2009; Tambini et al. 2010). Conversely, an individual's pattern of FC at rest predicts their performance on a subsequent task

(Baldassarre et al. 2012). Therefore, interactions between resting states and task states form a complete or closed cycle that may reflect the functional significance of spontaneous interactions between regions in everyday life: resting activity affects task-evoked neural activity and behavioral performance, which in turn affects resting FC through a Hebbian process (**Fig. 1a**). According to this conceptualization, resting-state activity provides a useful prior or scaffold of biological states that can be modified for performance of different tasks. A related conceptualization focuses on the 'internal' environment and posits that the spontaneous interactions between regions, as in resting FC, are due to connectivity patterns that are coded as synaptic efficacies in cortical networks and reflect an individual's cognitive traits or biases (Harmelech and Malach 2013; Strappini et al. 2018).

To evaluate these ideas, however, one must move beyond measures of overall FC between regions and instead test for the presence and connectivity of resting multi-voxel patterns that conform to the neural patterns associated with states of the internal and external environment. Multi-voxel analyses of fMRI task signals have shown that neural states or patterns of local activity during tasks do in fact carry information about stimulus categories, retrieved memories or cognitive processes such as attention (Haxby et al. 2001; Haynes and Rees 2005; Kamitani and Tong 2005; Kriegeskorte et al. 2006; Serences and Boynton 2007; Kriegeskorte et al. 2008; Greenberg et al. 2010; Kuhl and Chun 2014) and can be modulated by learning.

A representational function for resting activity might seem surprising since the brain appears capable of coding a huge, almost unlimited number of states. However, studies of the motor system indicate that the brain partly deals with the large number of

possible hand movements through synergies (Schieber and Santello 2004; Santello et al. 2013) that reduce dimensionality. Studies of human hand movements under experimental and naturalistic conditions (Santello et al. 1998; Ingram et al. 2008) have isolated a small number of principal components that code for large amounts of variance and distinguish a variety of movements. Moreover, a recent fMRI study reported that these components map onto multi-voxel patterns of movement-evoked BOLD activity in regions of motor and premotor cortex, SMA, SPL, and anterior IPS (Leo et al. 2016). The existence of these modal axes or synergies increases the plausibility that resting activity might encode these biologically important representations. A similar idea can be extended to other domains. For example, multi-voxel patterns in temporal-occipital cortex vary along general features of object categories such as animacy (Martin et al. 1996; Chao et al. 1999; Kriegeskorte et al. 2008; Sha et al. 2015) or, in literate adults, sensitivity to orthography (Cohen et al. 2000; Dehaene et al. 2004; Binder et al. 2006; Vinckier et al. 2007).

Here we tested the hypothesis that multi-voxel patterns of resting state activity in visual cortex are related to the multi-voxel patterns evoked by naturalistic (e.g. faces) and non-naturalistic (e.g. phase-scrambled faces) visual stimuli. We determined this relationship in high-level regions of visual cortex that show preferences for object categories, and are presumably sensitive to the higher-order features/statistics that define naturalistic objects. We also tested regions in early visual cortex that are more influenced by low-level features. These latter features occur in naturalistic objects but are also present in phase-scrambled and grid-scrambled objects in which the higher-order features/statistics that define natural categories have been removed.

Subjects received resting scans, localizer scans, and task scans. Localizer scans determined the tested ROIs and task scans identified the multi-voxel 'representational' patterns evoked by the different modal and non-modal object categories. These representational patterns were then correlated with the multi-voxel patterns measured on each frame of resting-scans. The resulting distribution of correlation coefficients indicated the extent to which resting activity patterns matched stimulus-evoked patterns.

We specifically contrasted whether resting state multivoxel patterns 1) corresponded better to multivoxel patterns evoked by some naturalistic or 'modal' object categories (e.g. faces) than others (e.g. tools) and/or 2) corresponded better to patterns evoked by modal object categories than non-naturalistic or 'non-modal' stimuli (e.g. phase-scrambled faces or tools). In addition, we determined whether resting activity patterns were better approximated by stimulus-evoked patterns that represented a category mean or prototype vs. stimulus-evoked patterns for individual exemplars of a category.

## Materials and Methods

### *Participants*

The study included 16 healthy young adult volunteers (10 female; age 21 – 35 years-old) with no prior history of neurological or psychiatric disorders. All participants were right-handed native English speakers with normal or corrected-to-normal vision. All participants gave informed consent to take part in the experiment, and the study was

approved by the Institutional Review Board (IRB) of Washington University in St. Louis School of Medicine.

***Stimuli***

Nine categories of color images subtending $8^o$ x $8^o$ of visual angle were included in event-related 'task' fMRI scans. Seven categories consisted of ecological or 'modal' images that are frequently encountered: human faces, human bodies, mammals, chairs, tools, scenes, and words. The categorical modal stimuli, excluding the word category, were obtained from Downing et al., 2006 (Downing et al. 2006). Faces, bodies and mammals served as animate categories, and chairs, tools and scenes as inanimate categories (Kriegeskorte et al*.* 2008). Word stimuli were included for exploratory analyses and results for those stimuli will not be considered in this paper.

Two control, non-ecological/non-modal stimulus categories were constructed from the modal stimuli used in the experiment, excluding the word stimuli. A low-level control consisted of phase-scrambled stimuli that preserved the spatial frequency amplitude spectrum of the modal images. An intermediate-level control consisted of grid-scrambled stimuli that included basic visual properties of the modal images such as line segments and connectors. For the low-level control condition, 2D phase scrambled images of the exemplars from the 6 categories were generated by applying the same set of random phases to each 2-dimensional frequency component of the original image while keeping the magnitude constant (Watson et al. 2016). Exemplars from all six modal categorical stimuli except real word stimuli were 2D phase scrambled, yielding a

total of 144 2D Phase scrambled stimuli. For the intermediate-level control condition, grid-scrambled images of exemplars from the six modal categories were generated by sub-dividing each image into a 10 x 10 grid (each grid is $0.8^o$ x $0.8^o$) and randomly rearranging the individual grid segments.

Color images of exemplars from seven categories were included in localizer scans: human faces, human bodies, objects (chairs and tools), scenes, words, false font character strings and phase scrambled images. The categories for the localizer scans differed slightly from the categories for the task scans since the former was only used to define the regions of interest (ROIs). ROIs related to the false font and word stimuli will not be considered in this paper.

Stimuli were presented using the Psychophysics Toolbox package (Brainard 1997) in MATLAB (The MathWorks). Stimulus images were projected onto a screen and were viewed through a mirror mounted on the head coil. All stimuli were presented centrally on a gray background.

### *Scanning Procedure*

The study consisted of two separate sessions, each conducted on a separate day. In session one, subjects received 3 resting state runs, 2 localizer runs, and 8 task runs. In session 2, subjects received 2 resting state runs, 2 localizer runs, 8 task runs, and 2 post-task resting state runs. One subject had a total of 13 task runs over the two sessions instead of 16 (**Fig. 1b**).

*Resting state runs.* Participants received a total of 7 resting state scans, each lasting 5 min (300 TRs). During a scan the participant was asked to maintain fixation on a cross that was displayed at the center of the screen during the entire run. Five resting scans (3 for first session and 2 for second session) were conducted before any localizer or task scans to collect stimulus-free intrinsic activities. For the second session only, two additional 5 min resting state scans were conducted after the task scans to investigate potential post stimuli-driven effects on intrinsic activity. The results from the post-task resting scans will not be discussed here.

*Localizer runs.* Each session included 2 localizer runs (4 in total), each lasting 5 min and 40s (340 TRs), and each localizer scan was presented in a blocked fMRI design. Each block of a localizer run contained 20 images of a single category, and those images were different from the images used in the task scans. A fully randomized sequence of eight blocks, consisting of the 7 stimulus categories and a fixation block, was repeated twice within each run. At the beginning and the end of each run, an additional fixation block was presented for 4s and 16s. Within each category block, images were presented for 300ms with an inter-stimulus interval (ISI) of 700ms. A fixation cross was continuously present at the center of the screen during the ISI and during fixation blocks. During category blocks, participants performed a minimally cognitively engaging task by pressing a button if the initially presented image was changed in size or position during the 300ms presentation.

*Task runs.* Each session included 8 task runs (16 in total), each lasting 5 min and 15s (315 TRs). For each subject and for each run, stimulus presentation order and inter-stimulus intervals were fully randomized using Optseq2 (Dale 1999). Each stimulus

presentation lasted for 300ms and the interval between stimuli was jittered between 3.7s and 8.7s. A fixation cross was continuously present at the center of the screen during the ISI. In each modal category, there were 24 separate exemplars (e.g. 24 different faces) and each exemplar was repeated 4 times. In each non-modal category, there were 96 exemplars, each presented once. Participants performed a minimally cognitively engaging task by pressing a button if the presented image changed its size or position during a 300ms presentation, the same task as that performed during the localizer scans.

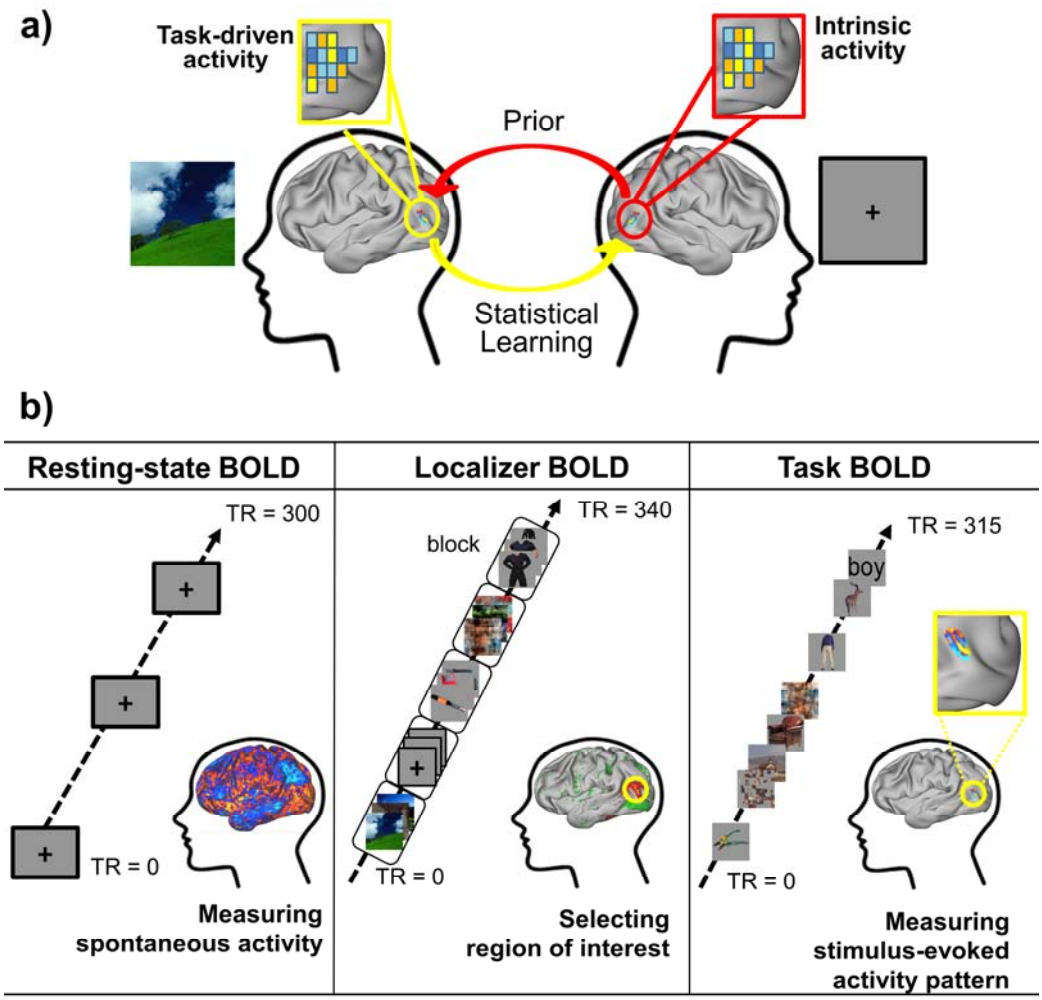


**Figure 1. (a)** The putative cyclic interplay between brain activity evoked by real-world experiences and resting-state activity. **(b)** Experimental design.

### *Imaging parameters*

Data were obtained from a Siemens 3T Prisma MRI scanner. Structural images for atlas transformation and lesion segmentation were acquired using T1-weighted magnetization prepared-rapid gradient echo (MP-RAGE) (1 x 1 x 1 mm voxels; echo time [TE] = 2.36 ms, repetition time [TR] = 1700 ms, TI=1000 ms, flip angle = 8°) and T2-weighted fast spin echo sequences (1 x 1 x 1 mm voxels; TE = 564 ms, TR = 3200 ms). FMRI scans were collected using a gradient echo-planar sequence sensitive to BOLD contrast (TE = 26.6 ms, flip angle = 58°, 2.4 x 2.4 x 2.4 mm voxels, 48 contiguous slices, TR = 1.0 s, and multiband factor of 4).

### *fMRI pre-processing*

fMRI data underwent pre-processing as previously described (Siegel JS et al. 2016). This included: (1) compensation for asynchronous slice acquisition using sinc interpolation; (2) elimination of odd/even slice intensity differences resulting from interleaved acquisition; (3) whole brain intensity normalization to achieve a mode value of 1000; (4) spatial realignment within and across fMRI runs; and (5) resampling to 2.4 mm cubic voxels in atlas space, including realignment and atlas transformation in one resampling step. Cross-modal (e.g. T2-weighted to T1-weighted) image registration was accomplished by aligning image gradients.

Surface generation and processing of functional data followed procedures similar to Glasser et al (Glasser et al. 2013). First, anatomical surfaces were generated for each subject's T1 MRI using FreeSurfer automated segmentation (Fischl et al. 1999). This step included brain extraction, segmentation, generation of white matter and pial surface, inflation of the surfaces to a sphere, and surface shape-based spherical registration to the subjects' "native" surface to the fs_average surface. The left and right hemispheres were then resampled to 164,000 vertices and registered to each other (Van Essen et al. 2001).

Data were passed through several additional preprocessing steps: (i) removal by regression of the following sources of spurious variance: (a) six parameters obtained by rigid body correction of head motion, (b) the signal averaged over the whole brain (global signal regression), (c) signal from ventricles and CSF, and (d) signal from white matter; (ii) temporal filtering retaining frequencies in the 0.009–0.08-Hz band; and (iii) frame censoring (framewise displacement (FD) ≥ 0.5mm). The first four frames of each BOLD run were excluded.

To account for magnitude variability between different task and resting state runs, the BOLD timeseries for each vertice were Z-normalized across time within the task and the resting state runs. This Z-normalization was not applied to the localizer scans. Also, it was not applied to the Task scans for a separate analysis described below in which task-evoked activation magnitudes were determined (see below, ***Task scans: multi-voxel activation patterns).***

***Defining ROIs from localizer activation contrasts***

ROIs were defined from univariate vertice-wise statistical contrasts on the localizer activation magnitudes for different categories. For example, face-selective areas were defined from the significant vertices for the contrast of faces minus objects, where objects consisted of chairs and tools. First, for each participant a general linear model (GLM) was applied to their functional localizer scans. The GLM consisted of separate regressors for each stimulus category (e.g. faces) using an assumed hemodynamic response function from the Statistical Parametric Mapping (SPM12), a baseline term, and a linear trend term. Condition contrasts were formed to identify vertices showing preferences for each category, using a scheme similar to that of Bracci and Op de Beeck (2016) (Bracci and Op de Beeck 2016): body-preferences (body > objects, i.e. chairs and tools), face-preferences (face > objects), scene-preferences (scene > objects), modal-preferences (face + body + scene + object > phase-scrambled), and non-modal-preferences (phase-scrambled > face + body + scene + object).

A group random-effect statistical Z-map for each contrast was then computed from the single-subject GLMs (see **Figure 2a** for the group z-statistic map for each contrast). The Z-values obtained were sorted in magnitude. From the highest Z-values from the map, the group peak with the next highest Z-value was generated until the Z-value was <= 2.0. Group peaks had to be separated by at least 38.4mm (9.6 mm x 4) in the sphere mesh to prevent a vertex being assigned to multiple ROIs in a subject. ROIs were then defined separately for each participant based on the individual's univariate statistical maps (Oosterhof et al. 2012; Wurm et al. 2016). From each group peak

defined above, the corresponding peak for an individual subject peak was defined as the vertex with the highest Z-value within a sphere of 9.6 mm radius centered around the group peak in each subject's sphere mesh. The single-subject ROI was formed from the vertices exceeding Z= 2.0 in a sphere of 9.6 mm radius centered around the peak in the subject's mesh. All ROIs used in following analysis contained at least 175 vertices in at least 14 subjects. ROIs in individual subjects with less than 175 vertices were discarded.

To remove differences in BOLD magnitude across MR frames, for each ROI a z-normalization was applied across the vertices of each frame of the resting and task scans. This within-frame Z-normalization was not applied to the localizer scans. Also, it was not applied to the Task scans for a separate analysis described below in which task-evoked activation magnitudes were determined (see below, ***Task scans: multi-voxel activation patterns)***

Two sets of ROIs were created for use in different analyses. The first set was created from the localizer-defined ROIs that preferred a particular target category (face, body, or scene) relative to the object category (chairs + tools). We grouped the vertices from the target-preferred ROIs into a single target-preferred joint-ROI. For each joint-ROI, all vertices located in early visual areas (V1 to V3) were excluded (Strappini et al. 2018), as estimated from surface topology using the template created by Benson et al. (Benson et al. 2012). A second set of ROIs consisted of Modal ROIs (face + body + scene + object > phase-scrambled) and Non-Modal ROIs (phase-scrambled > face + body + scene + object). Modal and Non-Modal ROIs were grouped, respectively, into a Modal joint-ROI and a Non-Modal joint-ROI. **Table S1** summarizes the mean MNI

coordinate, mean Z-score for the obtained group peak, and mean number of vertices for all constituent ROIs in each joint-ROI. **Figure 2b** schematically indicates the position of all constituent ROIs in a joint-ROI based on their group-peak locations. **Figure S1** shows the location of all Non-Modal ROIs superimposed on a surface map of V1-V3 using the template from Benson et al. (Benson et al. 2012).

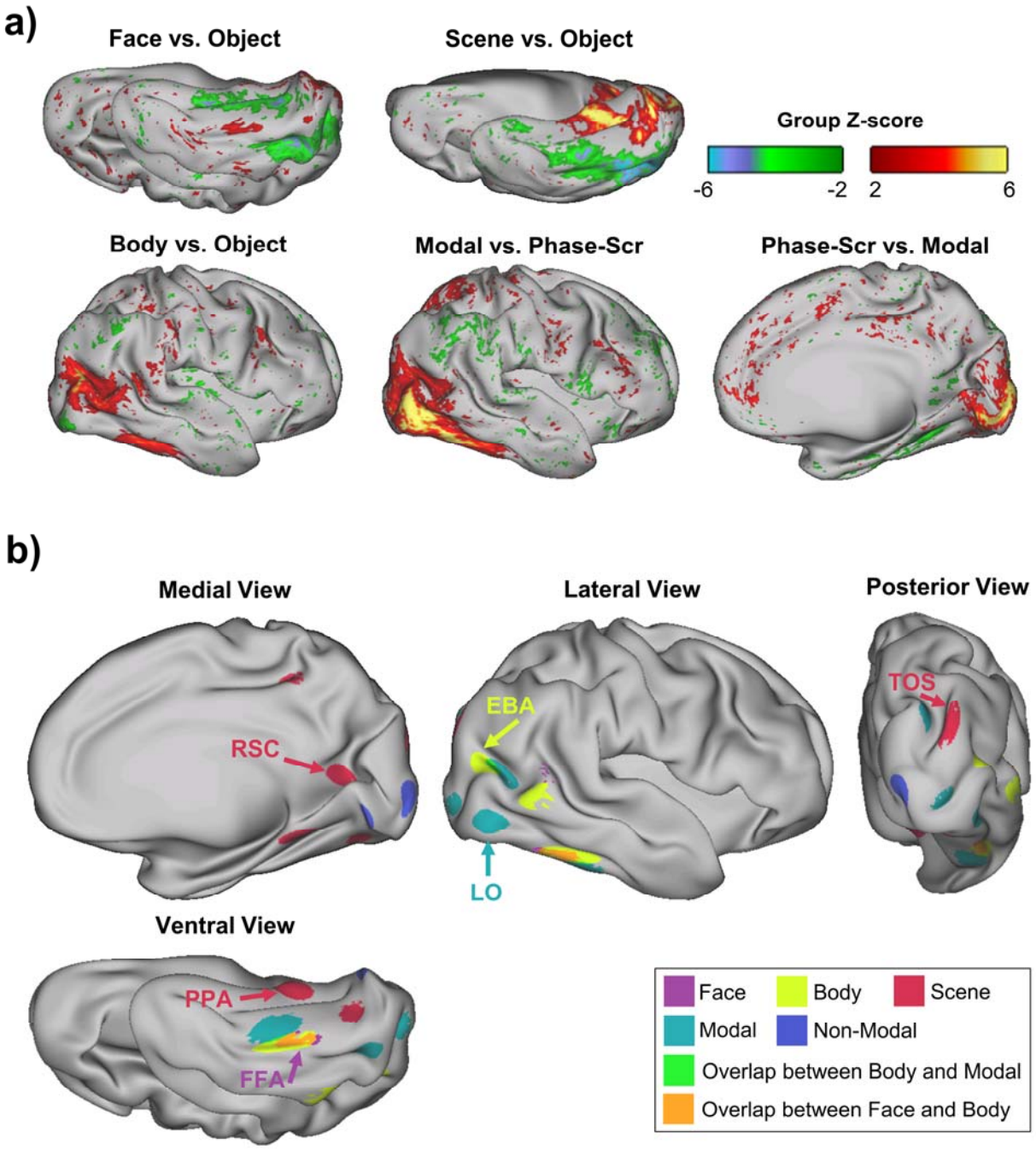


**Figure 2. (a)** Group z-statistic Localizer maps. ROIs were separately defined for individual from their localizer maps using the group foci as a constraint (see Methods, Defining ROIs from localizer activation contrasts). **(b)** Three sets of category-preferential ROIs were defined for faces, bodies, and scenes using the object category (tools and chairs) as the baseline. The ROIs in each set were combined into a joint-ROI after excluding regions in V1-V3 as determined from the Benson template

(Benson et al. 2012). Two additional sets of ROIs were defined by contrasting all modal categories (face, body, object, and scene) against the phase-scrambled condition. The positive contrast (i.e. face+body+object+scene > phase-scrambled) and negative contrast (i.e. face+body+object+scene < phase-scrambled) each yielded a set of ROIs that were combined, respectively, into a Modal joint-ROI and a Non-Modal joint-ROI. The locations of the constituent ROIs for each of the five joint-ROIs are schematically shown based on the group locations.

### *Localizer scans: multi-voxel activation patterns*

For each joint-ROI from each subject, the multi-vertex activation pattern for each stimulus category from the localizer scans was estimated. To accomplish this, a general linear model (GLM) was constructed using 7 category regressors, and baseline and linear trend regressors for each scan. Each category regressor was convolved with an assumed hemodynamic response function. The output localizer β weight matrix was a categorical multi-voxel pattern of size $N_c$ x $N_v$ ($N_c$ = Number of the localizer categories & $N_v$ = Number of vertices belong to the ROI). The mean localizer categorical activation magnitude across vertices (a vector of size $N_c$ x 1) was computed from the obtained categorical β weight matrix for each category.

### *Task scans: multi-voxel activation patterns*

For each Joint-ROI from each subject, the multi-vertex activation pattern for each of the 96 stimulus presentations for a category in the task scans was estimated via a GLM that included a separate regressor for each stimulus presentation (**Fig. 3**). In

addition, the GLM included a target regressor for the trials in which a stimulus was perturbed in size or position, and baseline and linear trend regressors for each scan. Each stimulus regressor was convolved with an assumed hemodynamic response function. The output task β weight matrix was a presentation-specific stimulus-evoked BOLD multi-voxel pattern of size $N_p$ x $N_v$ ($N_p$ = 96 presentations by category x 8 stimuli categories & $N_v$ = Number of vertices belong to the joint-ROI).

Two kinds of stimulus-evoked spatial patterns or templates were computed for each category and joint-ROI from the β weight matrix. An averaged stimulus-evoked pattern or prototype template was computed by averaging the β weights from all 96 presentations of a category at each vertex of the joint-ROI (red pattern in **Fig. 3a**; **Table S2** indicates the spatial correlation between the prototype templates for face, body, and scene in the three joint-ROIs**)**. A single-instance stimulus-evoked pattern or exemplar template was formed from the β weights for a single presentation from the category (magenta and green patterns in **Fig. 3b** indicate two exemplar templates**)**.

In order to determine mean task-evoked categorical magnitudes, a β weight matrix was separately computed using spatially non-normalized BOLD timeseries from the task scans. The mean task categorical activation magnitude for each category (a vector of size $N_c$ x 1) was computed by averaging the β weight matrix across vertices and presentations within a category.

***Determining similarity of resting multi-vertice patterns and stimulus-evoked patterns***

For each participant's individual joint-ROI, we determined the degree to which the multi-vertice pattern for a stimulus-evoked template for a category matched the multi-vertice pattern on each resting frame. In this procedure, illustrated in **Figures 3a** and **3b**, framewise intrinsic activity patterns were obtained from independent resting-state scans. Next, for the averaged stimulus-evoked pattern for a category (e.g. the prototype template for 'scene, **Fig. 3a**), the template spatial pattern was spatially correlated with the resting activity pattern on a frame. This procedure was repeated across all resting frames, resulting in a distribution of correlation coefficients (one coefficient per resting frame) for a particular category prototype in a particular joint-ROI. The upper 90% value of each distribution, hereafter termed the **U90-value**, was then determined. The U90 value computed for a prototype template served as a measure of the relationship between resting activity patterns and the patterns evoked by a category mean. For analyses that involved the Modal joint-ROI rather than joint-ROIs that preferred a particular category such as scene, U90-values for the six modal categories (face, body, mammal, chair, tool, scene) were averaged together to form a modal U90 value.

A similar procedure was applied to single instance stimulus-evoked patterns (e.g. exemplar templates for scene, **Fig. 3b**). Each exemplar template was spatially correlated with each resting frame to form a distribution of correlation coefficients for that template. The corresponding U90 value for the template was then determined. This procedure was applied separately to each of the ninety-six exemplar templates for a category, and the resulting ninety-six U90 values were averaged to arrive at a single

U90 value. This U90 value served as a measure of the average relationship between resting activity patterns and the patterns evoked by specific exemplars of the category.

Because the prototype template involved an average of ninety-six presentations and the exemplar template only one, the latter templates were noisier. However, each of the 24 exemplars from a modal category was repeated four times, enabling a second analysis that controlled for this factor. A ‘homogenous’ template was created for each of the 24 modal exemplars by averaging the β weights from the four presentations of each exemplar. As a control condition, a ‘heterogeneous’ template was created by averaging the β weights from single presentations of four different exemplars. A spatial correlation was computed between each template and each resting frame resulting in a distribution of 24 templates x #resting frames correlation coefficients based on homogenous or heterogeneous templates. A homogeneous and heterogeneous U90 value was then computed from the corresponding distribution.

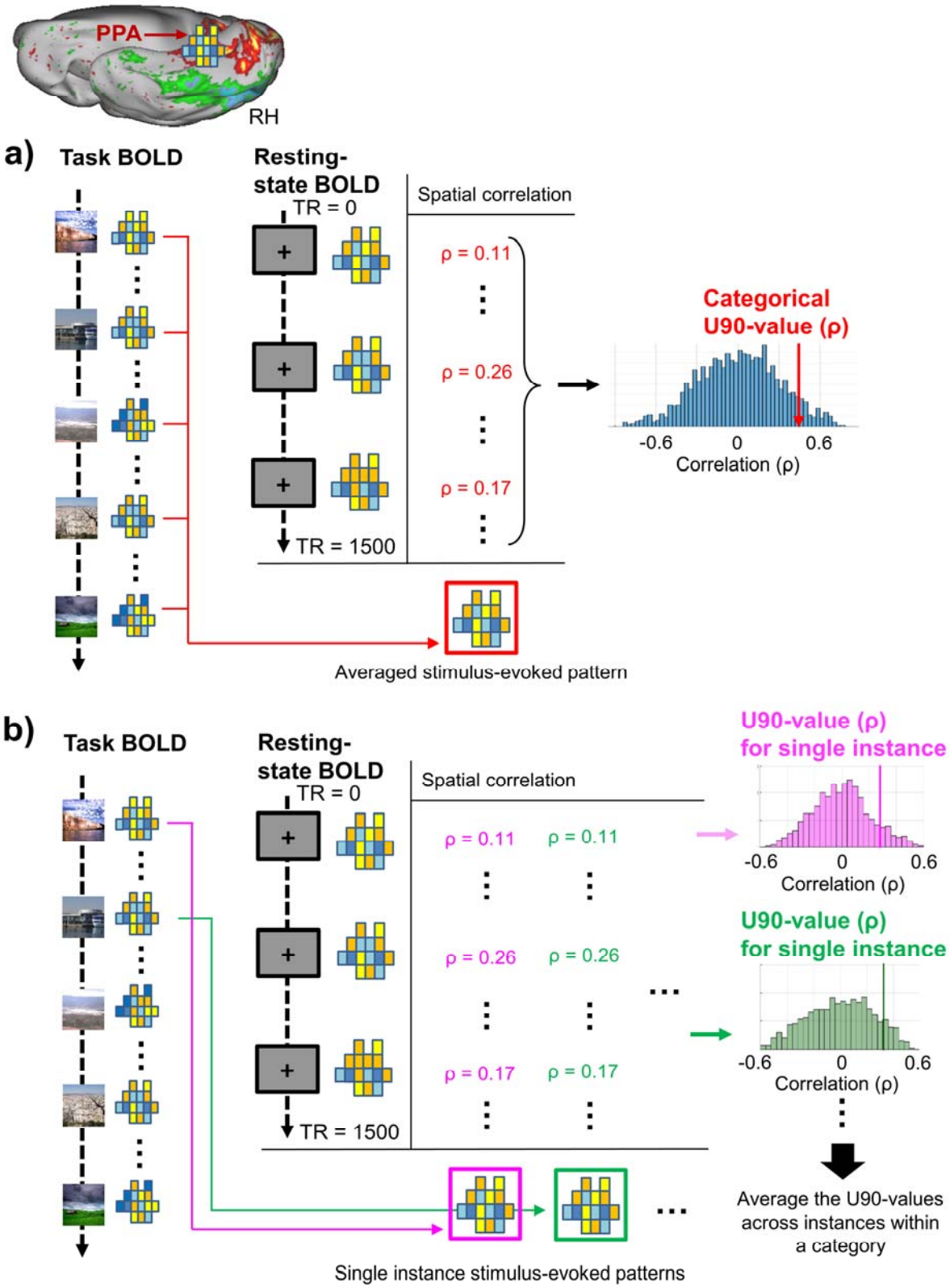


**Figure 3. (a)** Definition of U90-values using a prototype template. At each vertex of each joint-ROI, the β

weights for the 96 stimuli from each category were averaged, producing an averaged stimulus-evoked pattern or prototype template for each category and joint-ROI (e.g. the scene pattern outlined in red). For each joint-ROI, the spatial correlation between the prototype template and the resting activity pattern on a single resting frame was measured, yielding a spatial correlation coefficient for that frame. This procedure was repeated for all resting-state frames, yielding a distribution of spatial correlation coefficients. The upper 90% value from this distribution, shown by the vertical red arrow, was used as a summary measure of the distribution. **(b)** Definition of U90-values using exemplar templates. At each vertex of each joint-ROI, the β weights for a single stimulus presentation from a category comprised a single instance stimulus-evoked pattern or exemplar template for the category (e.g. the magenta pattern and green pattern represent two different exemplar templates for the scene category). For each joint-ROI, the spatial correlation between an exemplar template and the resting activity pattern on a single resting frame was measured, yielding a spatial correlation coefficient for that frame. This procedure was repeated for all resting-state frames, yielding a distribution of spatial correlation coefficients for the exemplar template. The upper 90% value from this distribution, shown by the colored vertical line, was used as a summary measure of the distribution for that exemplar. The average of all U90 values across exemplar templates yielded a summary U90 value.

### *Statistical analysis of U90 values*

U90 values were analyzed via repeated measures ANOVAs and paired t-tests. For example, the statistical significance of an overall dependence of U90 values for a joint-ROI on the stimulus category was determined by conducting repeated-measures ANOVAs with Category-Type as factors. Paired t-tests were conducted to test specific contrasts, with a Bonferroni-correction for multiple comparisons. For example, U90 values for modal vs. phase-scrambled stimuli were compared in the Modal joint-ROI.

## Results

The primary goal of the experiment was to compare multi-vertice activity patterns in the resting state to stimulus-evoked activity patterns from naturalistic (modal) and non-naturalistic (non-modal) stimuli. This comparison was conducted 1) in regions of higher-order visual cortex that preferred a particular modal category (e.g. faces) relative to other modal categories (e.g. objects), and 2) in regions of visual cortex that either preferred modal categories relative to the non-modal category of phase-scrambled objects or showed the reverse preference.

In the main analyses discussed below, the stimulus-evoked spatial pattern or template for a category was determined by averaging the β weights for the ninety-six stimulus presentations involving the category. Therefore, the stimulus-evoked template represented a category mean or prototype. In subsequent analyses, we also considered templates from specific exemplars of a category in order to determine if resting patterns of activity were better approximated by the prototype pattern or by patterns corresponding to specific exemplars.

The stimulus-evoked template for a category, whether a prototype or exemplar, was spatially correlated with the activity pattern in an ROI on each resting frame to determine a distribution of correlation coefficients over frames for the category and ROI (**Fig. 3)**. The upper 90% value (U90 value) of the distribution was then used as a summary measure of the relationship between the stimulus-evoked and resting patterns.

U90 values are sensitive to the mean, variance, and skewness of the underlying distribution of correlation coefficients. However, for all categories and ROIs, the distribution of correlation coefficients that defined the U90-value was symmetric and centered very near zero. **Figure 4a** shows the cumulative distribution for all subjects of spatial correlation coefficients across resting frames in face, body, and scene joint-ROIs for coefficients that were computed using the prototype face, body, and scene templates and the prototype phase-scrambled template. The distributions for modal and phase-scrambled stimuli were symmetric and centered on zero, but had different spreads. For the five joint-ROIs (Body, Face, Scene, Modal, Non-Modal) and eight stimulus categories (faces, bodies, mammals, tools, chairs, scenes, phase-scrambled, and grid-scrambled) the largest group averaged value of the distribution mean across the forty distributions of correlation coefficients was 0.011. Consequently, differences in U90 values between categories essentially reflected differences in the variance of the distributions of coefficients. In the results below, a larger U90 value indicates the presence of larger positive matches and negative matches of the resting pattern to the category-evoked pattern, rather than the (positive) degree of similarity.

***U90 values in joint-ROIs that prefer particular modal categories***

We conducted analyses that compared U90 values for a target category vs. other categories in individually-defined ROIs that preferred the target category, as determined by the localizer contrasts used to identify the ROIs. As an example, for the face target category preferred ROIs were defined from the localizer contrast face minus object.

Instead of analyzing each ROI separately, we grouped each set of category-preferential ROIs for an individual into a single joint-ROI. We then correlated the category template with the activity pattern on each resting frame across the entire joint-ROI, and derived a single U90 value for the target-preferred joint-ROI. ROIs in early visual cortex, as defined using the Benson template for V1 – V3 (Benson et al. 2012), were not included in category-preferential joint-ROIs, similar to the exclusion in (Strappini et al. 2018).

**Figure 4b** shows U90 values for a joint-ROI's target category (green symbol), non-target modal categories (red symbols), grid-scrambled category (blue symbol) and phase-scrambled category (gray symbol). Separate repeated measures analysis of variance (ANOVAs) for each joint-ROI with Category (8 levels) as a factor indicated a significant main effect of Category in all joint-ROIs (Face: $F(7,105)=10.3$, $p<.0001$; Body: $F(7,105)=10.8$, $p<.0001$; Scene: $F(7,105)=10.3$, $p<.0001$). The black symbols indicate significant differences in the U90 value for the joint-ROI's target category vs. each other category (paired t-tests; '+' = Bonferroni-corrected, $p<.05$, '++' = Bonferroni-corrected, $p<.005$, '*' = uncorrected, $p<.05$).

Within the face and body joint-ROIs, U90 values were larger for the joint-ROI's target category than for inanimate categories (chair, tool, scene) as well as for grid- and phase-scrambled objects. Within the scene joint-ROI, U90 values were larger for scenes than for all modal categories except chair, and were not much larger than the U90 values for the non-modal categories. These results demonstrate that in higher-order visual regions that showed stimulus preferences for a particular category, U90 values were larger for the preferred modal category or groupings of modal categories (e.g. animate categories) than for other modal and/or non-modal categories.

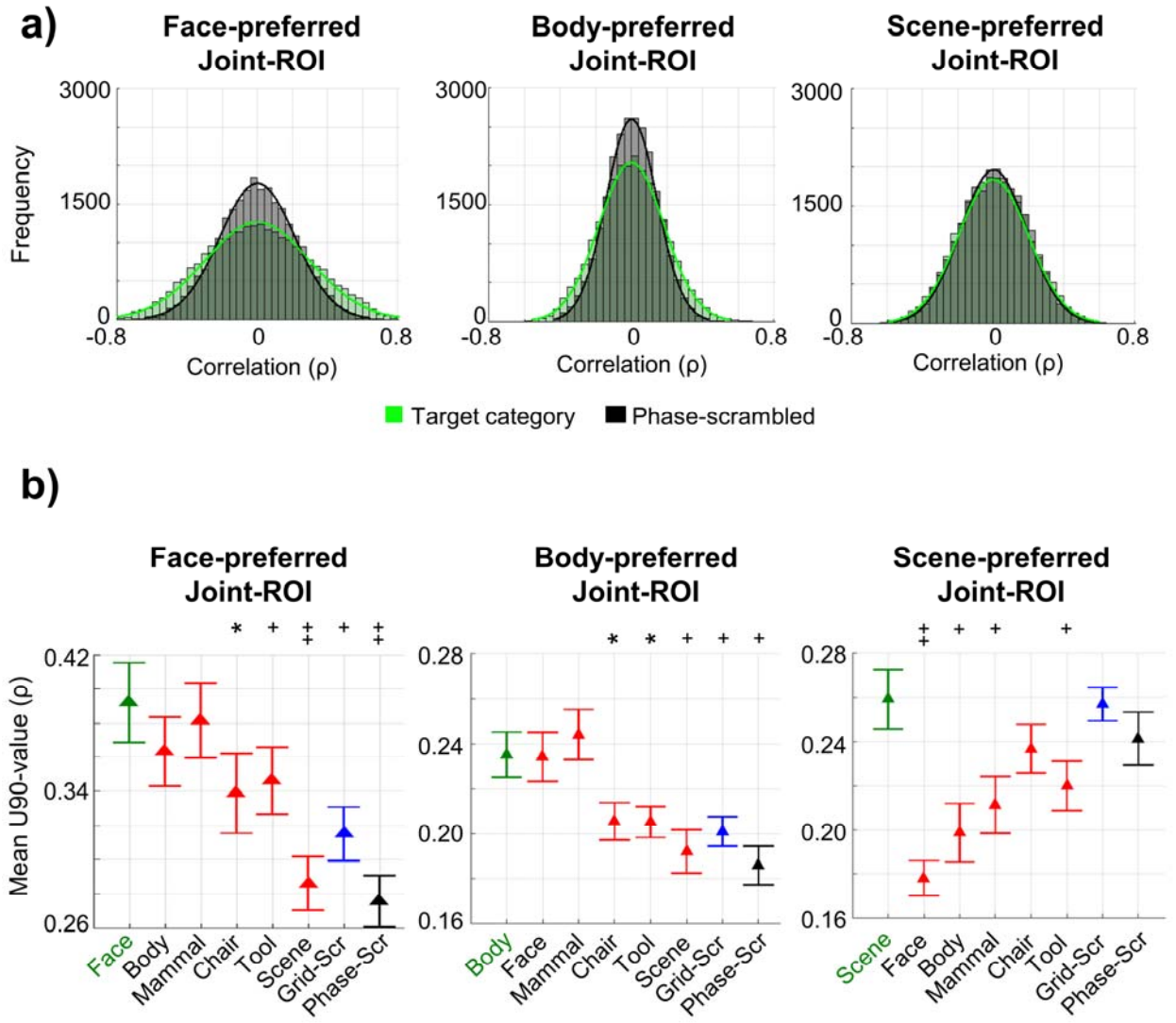


**Figure 4. (a)** Each graph shows for a joint-ROI the superimposed distributions of correlation coefficients between stimulus-evoked and resting activity patterns over frames for the joint-ROI's target category (light green; e.g. Face in the Face-preferred joint-ROI) and for the phase-scrambled category (gray). The stimulus-evoked template for a category corresponded to a 'prototype template' (procedure outlined in **Fig. 3a**). Overlapping sections of the two distributions are shown in dark green. The green and black lines have been fit to the distributions for the target and phase-scrambled categories, respectively, using the MATLAB program function 'fitdist.m'. **(b)** Group-averaged U90 values for categories in preferred vs. non-preferred joint-ROIs. For each of three joint-ROIs, the graph plots U90 values for the joint-ROI's target category (green symbol; e.g. U90 values for the face joint-ROI), non-target modal categories (red symbols), grid-scrambled category (blue symbol),

and phase-scrambled category (gray symbol). Significance of a group paired t-test comparing the U90 values within the preferred joint-ROI for the target category vs each non-target category is indicated by black symbols (+ = Bonferroni-corrected p-val ≤ 0.05; ++ = Bonferroni-corrected p-val ≤ 0.005; * = uncorrected p-val ≤ 0.05).

### *U90 values in joint-ROIs that prefer modal or non-modal categories*

The above analysis focused on joint-ROIs that showed preferential responses to a specific naturalistic category relative to other naturalistic categories (e.g. faces vs. chairs+tools). We also analyzed Modal and Non-Modal joint-ROIs in which stimulus-evoked responses were stronger or weaker for modal stimulus categories (face+body+scene+object) than phase-scrambled objects. Modal ROIs were located in lateral and ventral visual cortex while Non-Modal ROIs were located in medial visual regions (**Fig. 2** and **Fig. S1**).

**Figure 5** shows that in the joint-Modal ROI, the mean U90 value was larger for modal than phase-scrambled objects but not grid-scrambled objects, which contained visual features such as contours, line terminators and junctions. Therefore, when higher-level visual regions were not segregated by category preferences, resting activity did not necessarily differentiate between naturalistic objects and non-naturalistic objects that included lower-level visual features. The reverse pattern was observed for the joint-Non-Modal ROI, with higher U90 values for grid- and phase-scrambled objects than naturalistic objects. Therefore, U90 values in early visual cortex were larger for these non-naturalistic objects.

Confirming the above observations, an ANOVA with ROI-type (Modal, Non-Modal) and category (modal, grid-scrambled, phase-scrambled) as factors yielded a significant main effect of Category ($F(2,30)=9.92$, $p<.0005$) and a significant interaction of ROI-type by Category ($F(2,30)=12.9$, $p<.0001$). A sub-ANOVA with ROI-type (Modal, Non-Modal) and category (modal, phase-scrambled) also yielded a significant interaction ($F(1,15)=12.9$, $p<.005$), indicating that the critical interaction was not driven by the grid-scrambled objects.

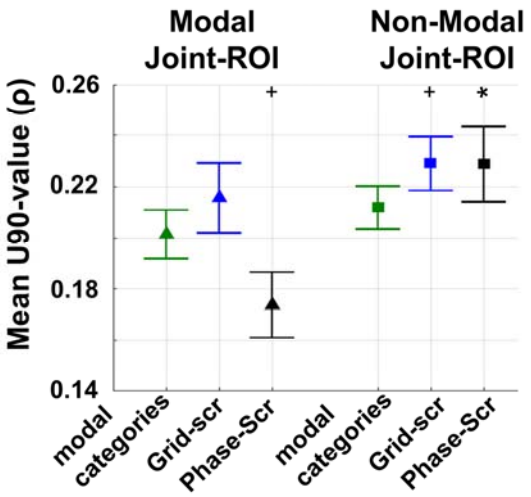


**Figure 5**. Group-averaged U90 values in Modal and Non-Modal joint-ROIs are plotted for modal and non-modal (phase-scrambled, grid scrambled) categories. Black symbols indicate significant differences between the modal category and each of the scrambled categories as determined by a group paired t-test (+ = Bonferroni-corrected p-val ≤ 0.05; ++ = Bonferroni-corrected p-val ≤ 0.005; * = uncorrected p-val ≤ 0.05).

### *U90 values correlate with activation strength and exemplar pattern similarity*

The previous analyses have shown that resting activity patterns showed higher U90 values for the patterns evoked by stimulus categories, whether modal or non-modal, which best activated the corresponding joint-ROI. **Figure 6** shows for Face, Body, Scene, Modal, and Non-Modal joint-ROIs the mean activation strengths during the Task (first column) and Localizer (second column) scans for each category, as defined from the β weights for the category averaged over subjects and the vertices of each joint-ROI. The task β weights used for the activation strength computation were separately computed from spatially non-normalized task BOLD timeseries (see Methods). The activation strengths in both the Task and Localizer scans followed the general pattern expected from the Localizer contrasts used to define the joint-ROIs, with the Task data independent of the Localizer data.

To determine whether the U90 value for a category and joint-ROI was related to the category's activation strength, for each subject and each joint-ROI, we computed the correlation coefficient across categories between the U90-value computed from the resting frames and the activation strength in the task or the localizer conditions. The group average correlation coefficient between U90 values and activation strengths for each Joint-ROI is shown in **Figure 6** (third column). Group one-sample t-tests indicated that the correlation coefficients were significant for both task and localizer scans in all Joint-ROIs except the Non-Modal joint-ROI. These results demonstrate that larger U90 values for a category in an ROI were generally related to how strongly the category activated the ROI.

The U90 values computed from the prototype templates for a category were also related to the degree to which the single-presentation (exemplar) templates from the

category were spatially correlated. We determined the average spatial correlation between the activity patterns from all pairings of stimulus presentations for a category (the 'exemplar template correlation value'), and then correlated this value with the corresponding U90 value across all categories. The correlation (**Fig. S2,** red symbols) was positive for all joint-ROIs, indicating that greater spatial similarity between the exemplar templates for a category was associated with larger U90 values. In addition, within each joint-ROI, larger exemplar template correlation values were associated with larger activation strengths (**Fig. S2**, black symbols). For this latter analysis, activation magnitudes were calculated using non-normalized timeseries while the templates that were spatially correlated with resting activity were computed using normalized timeseries (see Methods). Therefore, U90 values for a category were determined by two related factors: how well stimuli from the category activated an ROI and how strongly the single-presentation templates corresponding to those stimuli were spatially correlated.

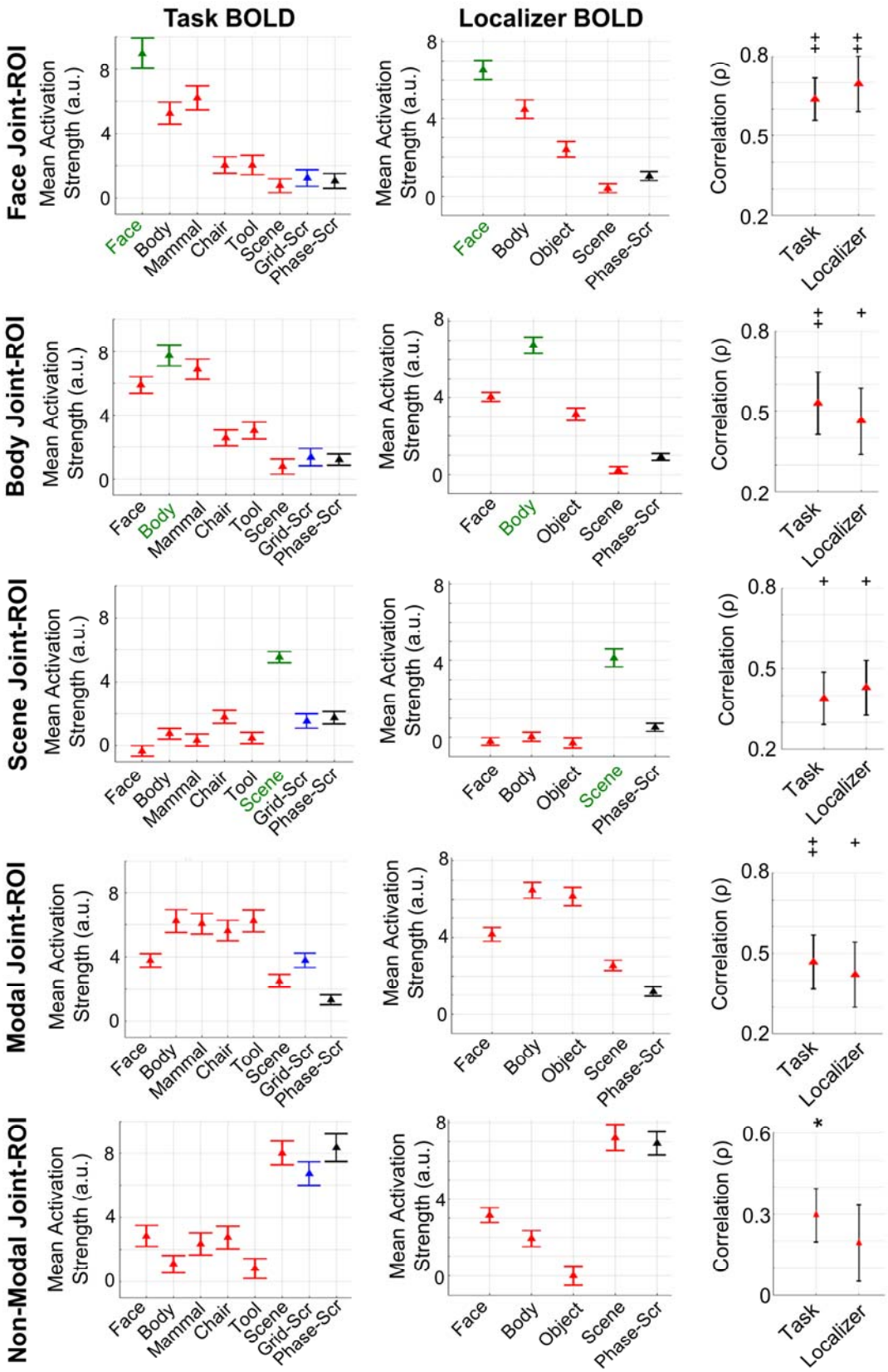
Task BOLD
Localizer BOLD
Face Joint-ROI
Body Joint-ROI
Scene Joint-ROI
Modal Joint-ROI
Non-Modal Joint-ROI
Mean Activation Strength (a.u.)
Correlation (ρ)
Face
Body
Mammal
Chair
Tool
Scene
Grid-Scr
Phase-Scr
Object
Task
Localizer

**Figure 6**. The correlation between U90 values and activation strengths. The mean activation strength in Face, Scene, Body, Modal, and Non-Modal joint-ROIs from the task and localizer scans for all stimulus categories are plotted for in the first and second columns, respectively. The correlation between activation strengths and U90 values across all categories is shown for both task and localizer scans in the third column. Black symbols indicate the significance of each correlation coefficient, as determined by a group 1-sample t-test (+ = Bonferroni-corrected p-val ≤ 0.05; ++ = Bonferroni-corrected p-val ≤ 0.005; * = uncorrected p-val ≤ 0.05).

### *U90 values for exemplar templates*

The results shown in **Figures 4, 5,** and **6** were based on stimulus-evoked templates that were formed by averaging the activity across individual stimulus presentations. Therefore, the template reflected a category average or prototype.

However, the spontaneous activity at a timepoint may reflect exemplars of the category from different parts of the category's feature space rather than a category average. Therefore, we also calculated U90 values for exemplar templates that were based on a single stimulus presentation from a category (**Fig. 3b**). For each exemplar template, we computed the spatial correlation coefficient between the template and each resting frame, producing a distribution of correlation coefficients for that template, as shown in **Figure 7a**. We then calculated the U90 value for the template and repeated the procedure for each of the ninety-six stimulus presentations for a category. Finally, we averaged the U90 values that were computed from the ninety-six exemplar templates to arrive at a single U90 value. If resting activity patterns match different

exemplar templates at different points in time, then the U90 value calculated from this procedure should be larger than the U90 value calculated using prototype templates.

The procedure using exemplar templates yielded U90 values for preferred and non-preferred stimuli that differed modestly in magnitude (**Fig. 7b)**. A 1-factor ANOVA, however, indicated a significant main effect of Category (8 levels) for all three joint-ROIs (Face: $F(7,105)=10.2$, $p<.0001$; Body: $F(7,105)=7.51$, $p <.0001$; Body: $F(7,105)=3.17$, $p<.005$), and paired t-tests indicated differences for each joint-ROI between the target category and some non-target categories.

Differences in U90 values between categories were more marked for prototype templates than for exemplar templates (i.e. compare **Fig. 4b** and **Fig. 7b**). Separate 2-factor ANOVAs on U90 values in the face, body, and scene joint-ROIs were conducted with Template-type (prototype, exemplar) and Category-type (8 levels) as factors. For all three joint-ROIs, the main effect of Template-type was significant (face: $F(1,15) = 678.6$, $p<.0001$); body: $F(1,15) = 1033.1$, $p<.0001$); scene: $F(1,15) = 1381.9$ , $p<.0001$), confirming larger U90 values for prototype templates, and the main effect of Category-type was significant (face: $F(7,105) = 17.0$, $p<.0001$); body: $F(7,105) = 18.8$, $p<.0001$); scene: $F(7,105) = 12.3$ , $p<.0001$). The interaction of Template-Type x Category-Type was significant for the Face joint-ROI ($F(7,105) = 2.295$, $p=.032$) and the Scene joint-ROI ($F(7,105) = 7.575$, $p < .0001$), confirming that in those joint-ROIs, differences in U90 values between categories were larger for prototype than exemplar templates.

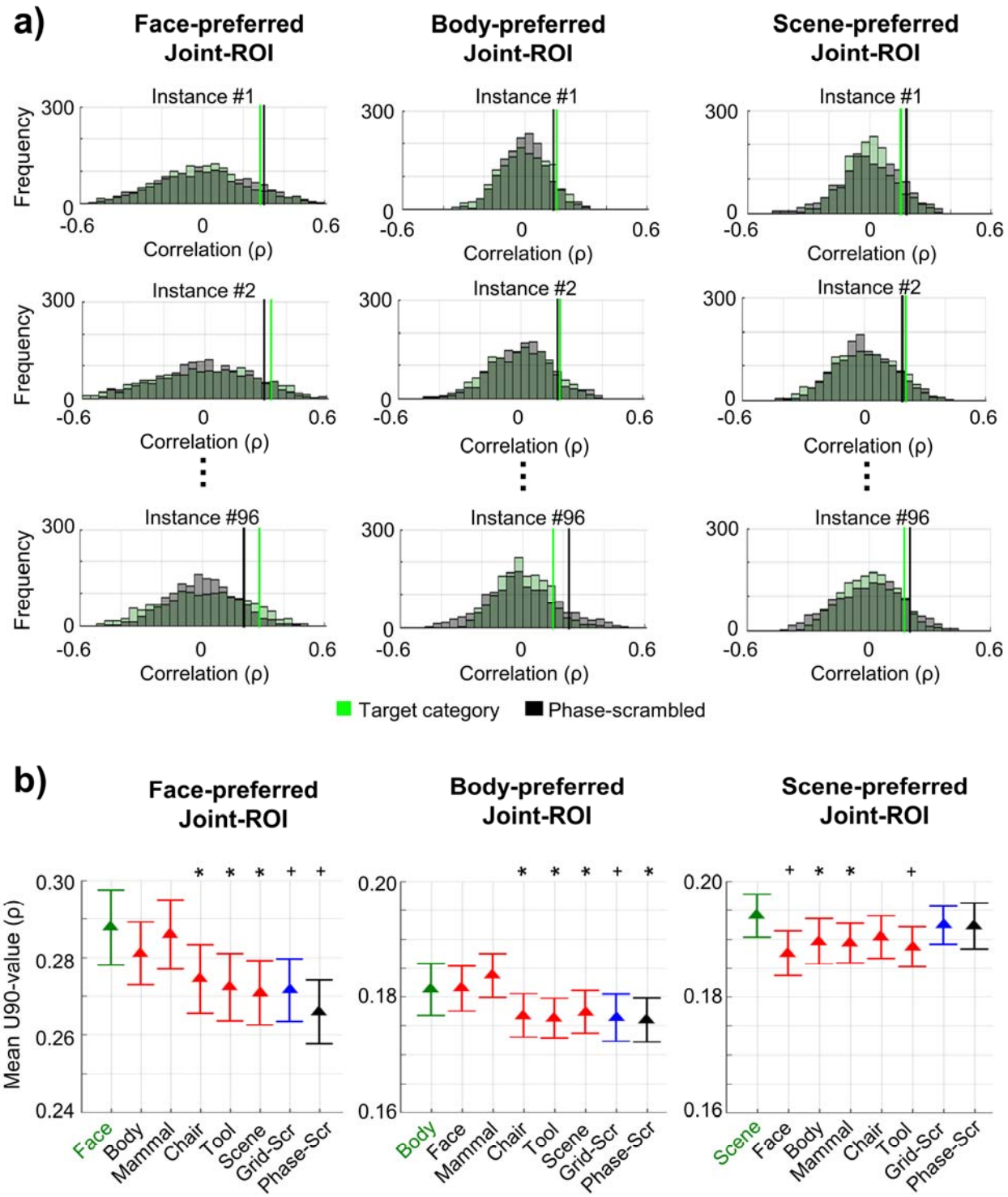


**Figure 7. (a)** Distributions of correlation coefficients for exemplar templates. The graphs show for a single subject the distribution across resting frames of the spatial correlation coefficient between templates for single instances of a category (exemplar templates; **Fig. 3b**) and the resting activity pattern on a

frame for the joint-ROI's target category (green) and for the phase-scrambled (grey) category. Overlapping sections of the two distributions are shown in dark green. The green and black vertical lines show the U90 values for the target and phase-scrambled categories, respectively. **(b)** U90 values for a joint-ROI's target category (green symbol), non-target modal categories (red symbols), and grid-scrambled (blue symbol) and phase-scrambled (black symbol) categories. Black symbols indicate the significance of group paired t-tests between the U90 values for the target category and each other category (+ = Bonferroni-corrected p-val ≤ 0.05; ++ = Bonferroni-corrected p-val ≤ 0.005; * = uncorrected p-val ≤ 0.05).

We conducted a second test of whether the relationship between resting activity and category-evoked templates reflected activity patterns for specific exemplars of the category or prototype patterns that generalized over exemplars. An exemplar-specific template was created by averaging the four presentations of the same exemplar from a category, yielding 24 'homogeneous' templates. Each of the 24 templates was spatially correlated with the resting activity pattern on each frame, resulting in a distribution of correlation coefficients involving homogenous templates. We also created 24 'heterogeneous' templates by averaging a single presentation of four different exemplars. Again, each of the 24 templates was spatially correlated with the resting activity pattern on each frame, resulting in a distribution of correlation coefficients that involved heterogeneous templates.

**Figure 8a** shows the distributions of correlation coefficients for the preferred category in face-, body-, and scene-preferred joint-ROIs, as computed using homogeneous or heterogeneous templates. The distributions and corresponding U90 values for homogeneous templates, colored in magenta, and heterogeneous templates,

colored in green, were very similar (**Fig. 8b**). Paired t-tests indicated no differences in U90 values between the two templates for faces but weakly significant differences for bodies (t(15)=2.125, p=0.051, uncorrected) and scenes (t(15)=2.173, p=0.046, uncorrected). The latter result may partly reflect the fact that scene exemplars themselves were quite variable relative to face exemplars. For example, all face stimuli were in frontal view with a neutral face expression while the scene stimuli included both man-made scenery (e.g. buildings) and natural scenery taken from very different environments (e.g. pasture, desert, mountain, and ocean).

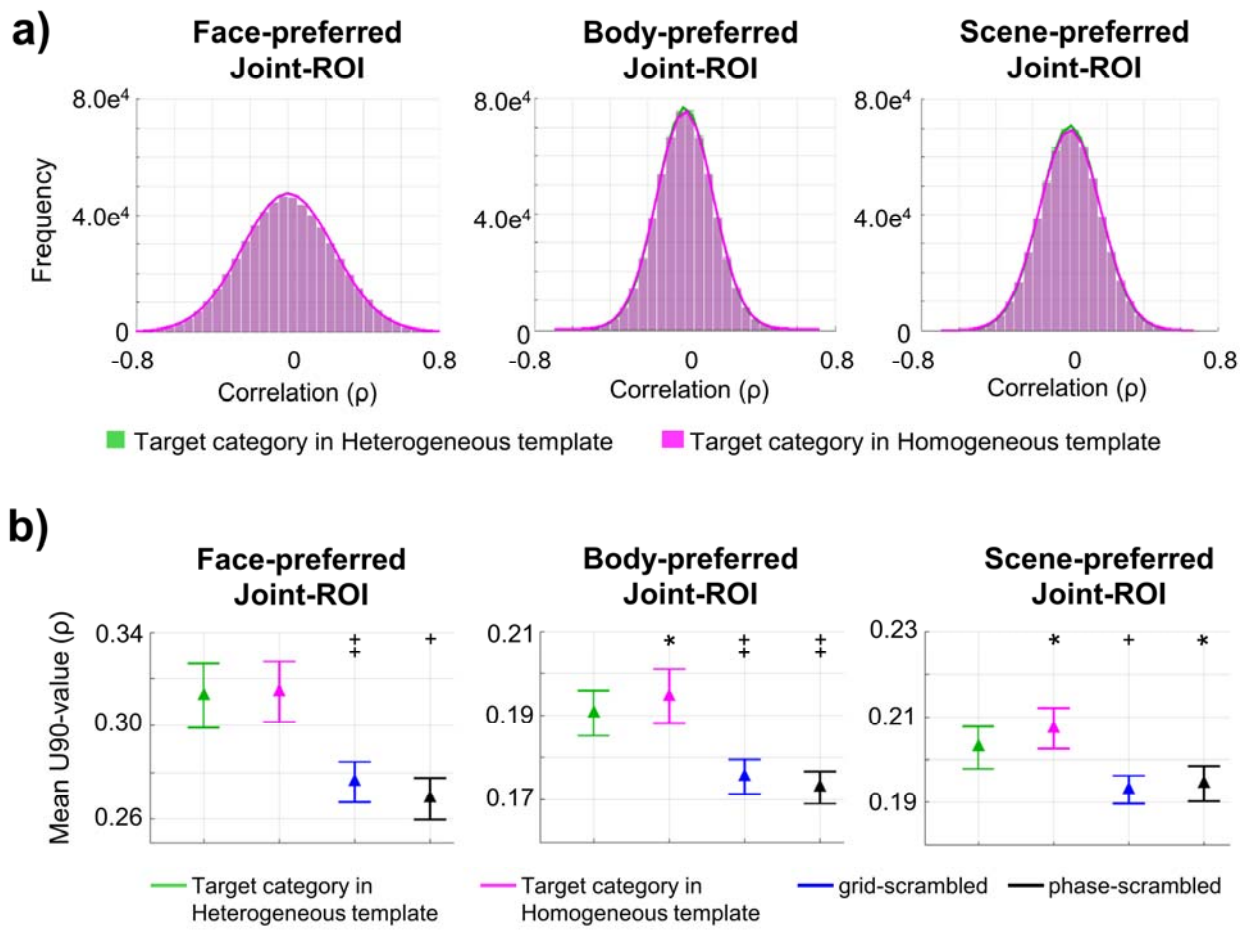


**Figure 8. (a)** Distributions of correlation coefficients from homogenous and heterogeneous templates. For each category, 24 homogenous templates were computed by averaging the four presentations of

the same exemplar for a category and 24 heterogeneous templates were computed by averaging a single presentation of four different exemplars. A single correlation coefficient was computed between each category template and each resting frame. From the distribution of coefficients across all 24 homogenous or heterogeneous templates for the category and all resting frames, the corresponding homogenous or heterogeneous U90 value was determined. The distributions of correlation coefficients based on homogenous and heterogeneous templates are almost completely superimposed (the green and pink outlines of the distributions determined by the MATLAB program function 'fitdist.m'). **(b)** U90 values for the homogenous-target, heterogeneous-target, phase-scrambled and grid-scrambled categories are shown from three joint-ROIs. Black symbols indicate the significance of paired t-tests comparing U90 values for the heterogeneous condition against each of the other three conditions (+ = Bonferroni-corrected p-val ≤ 0.05; ++ = Bonferroni-corrected p-val ≤ 0.005; * = uncorrected p-val ≤ 0.05).

Because each exemplar was only presented four times, the comparison of homogenous vs. heterogeneous templates was restricted in power. However, the results converged with those above showing greater variation in U90 values with category-average than exemplar templates. Therefore, the available evidence is most consistent with the view that U90 values in the tested ROIs mainly reflected categorical patterns that generalized over exemplars.

***Coherence of stimulus specific resting multi-voxel patterns in different regions of a joint-ROI***

The fact that U90 values in joint-ROIs were larger for preferred than non-preferred stimuli raises the possibility that at each resting timepoint, there existed a

spatially coherent brain state that extended across the constituent ROIs of the joint-ROI showing a common stimulus preference. Alternatively, if at each timepoint, the spatial match between the preferred-stimulus template and the resting activity pattern in a constituent ROI had varied independently across ROIs, then positive and negative correlations with the evoked template in different constituent ROIs would have cancelled, leading to a large reduction in the variance of the underlying coefficient distribution for the joint-ROI.

To assess whether constituent ROIs of a joint-ROI were spatially coherent, we simulated the U90 value for a joint-ROI under the assumption that resting patterns in the constituent ROIs fluctuated independently. To this end, the following procedure was conducted for each subject, joint-ROI, and category template. First, for each constituent ROI of a joint-ROI we randomly sampled a value from the empirically observed distribution of spatial correlation coefficients from that ROI for the match between the resting activity pattern and the category template. The values from the constituent ROIs were then Fisher transformed, averaged, and reverse Fisher transformed to yield a single value of the correlation coefficient distribution for the joint-ROI under the assumption that the resting state activity patterns in the constituent ROIs fluctuated independently. This procedure was then repeated 1.5 million times to fill out the simulated distribution. Finally, we determined the U90 value for the simulated distribution and compared it via paired t-test to the U90 value from the empirically determined U90 distribution for the joint-ROI.

For the preferred stimulus category within the corresponding joint-ROI (Face, Body, Scene), U90 values were significantly larger for the empirically observed

distribution than for the simulated distribution that assumed independence ($p<.0001$ in all cases; **Fig. S3**). This analysis demonstrates a non-zero degree of spatial coherence between constituent ROIs, although it does not determine the magnitude of this coherence. We conclude that at single points in time during a resting scan the spatial patterns in the constituent ROIs of a joint-ROI that preferred a particular stimulus category were coherent rather than independent. In other words, the spatial pattern of resting-state activity in a joint-ROI formed a distributed, linked brain state.

## Discussion

The goal of the experiment was to determine in regions of visual cortex the relationship between resting multi-vertice activity patterns and the multi-vertice patterns evoked by naturalistic and non-naturalistic visual stimuli. To this end, the multi-vertice patterns of the evoked BOLD activity from common 'modal' objects and from non-naturalistic or 'non-modal' stimuli such as phase-scrambled and grid-scrambled objects were correlated with resting multi-vertice patterns in brain regions independently defined using standard localizers.

The overall result, discussed in more detail below, is that on average, resting activity patterns in regions of visual cortex were not more similar to the pattern evoked by one stimulus category than another. Instead, stimulus-evoked patterns differed in the spread of positive and negative matches with resting activity patterns, as indexed by the U90 value (**Fig. 4**), The spread of match values was determined by how well a stimulus

activated the region, largely irrespective of whether that stimulus was naturalistic or non-naturalistic.

Therefore, the spatial pattern of resting activity in a distributed set of regions varied over frames along an axis that was best aligned with the spatial pattern of the regions' preferred stimulus, i.e. an axis with the two endpoints, preferred-stimulus and not-preferred-stimulus. In regions of high-level visual cortex showing modal category preferences, U90 values were higher for the regions' preferred modal category (**Fig. 4b**). In regions of early visual cortex, which were more strongly activated by non-modal categories such as grid-scrambled or phase-scrambled objects than by 'single-object' modal categories (face, body, mammal, chair, tool, but not scene; **Fig. 6**), U90 values were greater for the preferred non-modal stimuli (**Fig. 5**).

Finally, resting activity patterns in the constituent ROIs of a joint-ROI were not independent on a frame, but tended toward similar locations on the preferred-stimulus/not-preferred-stimulus spatial axis. Therefore, on each frame the constituent ROIs formed a coherent, linked brain state that was aligned positively or negatively with a stimulus-evoked representation.

Overall, these results are consistent with a general framework in which resting multivoxel patterns of activity within a brain region are affected by the past history of activity patterns evoked by the external and internal environment (Fiser et al. 2010; Harmelech and Malach 2013). The also show that resting activity patterns can potentially serve a representational function. However, they do not fit a conceptualization in which resting activity patterns are necessarily more similar to the

patterns evoked by a region's preferred stimulus. Instead, a region's stimulus preferences determine an axis along which the resting pattern maximally varies, and links the region's multi-vertice pattern to the multi-vertice patterns of regions that show similar preferences.

***Low- and high-level visual correspondences at rest***

Resting multivoxel patterns in visual areas were not necessarily related to the patterns evoked by naturalistic objects, since larger U90 values were observed in early visual cortex for grid-scrambled and phase-scrambled objects than for modal objects (**Fig. 5**). Instead, the relationship between spatial patterns of resting and stimulus-evoked activity in a region was more generally related to a region's stimulus preferences, i.e. to the stimuli that optimally activated the region. In many higher-level visual ROIs (**Fig. 4b**), these preferences favored particular naturalistic categories over other naturalistic categories or non-naturalistic categories. However, in early visual cortex, these preferences favored stimuli that weighted low-level features (**Fig. 5**). Grid-scrambled stimuli likely included a higher density of contours and line terminators/connectors/junctions than the original naturalistic images, while phase-scrambled images contained dense textures. Both features were also present in scene images (e.g. heterogeneous arrays of multiple small objects, wheat fields, clouds). Correspondingly, in the scene joint-ROI, phase-scrambled and grid-scrambled objects showed relatively high U90 values with respect to most single-object modal categories (**Fig. 4b**).

The larger U90 values for non-modal stimuli in early visual cortex do not contradict an overall framework in which resting activity patterns reflect the statistical distribution of features in the environment. Rather, this result suggests that resting activity patterns in regions that primarily extract low-level visual features are relatively independent of the patterns associated with higher-order features/statistics that define categories of naturalistic objects.

The results for grid-scrambled objects were particularly intriguing. Not only did grid-scrambled objects show greater U90 values than the modal category in early visual cortex (**Fig. 5)**, but in addition grid-scrambled and modal categories showed equivalent U90 values in the joint-Modal ROI (**Fig. 5)**. This equivalence may have reflected the fact that the union of different category-preferential regions in the joint-Modal ROI eliminated or reduced the importance of features selective for a particular naturalistic category. Instead, the U90 value reflected features common to different naturalistic categories that were also present in grid-scrambled objects.

Therefore, the distribution of matches between resting and evoked activity patterns can be driven by a variety of stimulus features that reflect local (e.g. contour-related features) or global (e.g. faces) stimulus characteristics depending on the tested region.

***Resting activity as a context-independent prior***

The rationale for postulating a representational function of resting activity is that limits on the information processing capacity of the brain may be mitigated by the

incorporation of useful prior information. Appropriate priors will generally depend on context and therefore will change dynamically. The perceptual priors appropriate to walking alone through a forest vs. eating a family meal at the dinner table are quite different. These putative dynamic changes are thought to reflect generative models of the expected input via top-down pathways (Mumford 1992).

Resting scans are usually conducted under conditions in which subjects lie in a dark tube while fixating a cross in an otherwise blank display, which would not seem a fertile context for a perceptual prior. However, some aspects of an appropriate prior may not heavily depend on context. Under the hypothesis that stimulus tunings reflect the statistical distribution of features in the environment (Fiser et al. 2010), perhaps coupled with additional constraints such as sparsity (Olshausen and Field 1996), the activation pattern corresponding to a region's stimulus preference may serve as an appropriate context-independent prior for a region. In addition, utility might be maximized for a system by including category preferential areas that require less stimulus evidence to generate stimulus-evoked representations of biologically important categories. A category-appropriate resting pattern could provide an appropriate ongoing bias. However, in category-preferential regions we found increases in the variance but not the mean of the spatial match between resting and evoked activity.

An alternative hypothesis is that the increase in variation for a region along the preferred-stimulus/not-preferred-stimulus pattern axis is related to the critical dynamics of the region. Criticality refers to a state whose dynamics enables a transition to a different state(s) in response to a small perturbation, as in a phase transition. Prior studies have suggested that resting activity conforms to critical states that are easily

perturbed by stimulus or task inputs (Deco and Jirsa 2012; Tagliazucchi et al. 2012; Chialvo 2010). The alignment of spatial resting patterns along the preferred stimulus/not preferred stimulus axis for a region, coupled with criticality, may better enable departures from the resting state along that axis and lead to better or faster discrimination along that axis. The axis itself may be determined by the joint influences of structural connectivity and resting functional connectivity (FC). Category specific activations are related to distinct structural connectivity fingerprints (Saygin et al. 2011; Osher et al. 2016), while recent studies have demonstrated mappings between resting FC and voxelwise activation patterns (Cole et al. 2016; Tavor et al. 2016). Resting FC is influenced not only by structural connectivity (Honey et al. 2009) but also by prior experience (Albert et al. 2009; Hasson et al. 2009; Lewis et al. 2009; Tambini et al. 2010), the latter effect thought to be mediated by changes in synaptic weightings.

The description of the poles of the axis of maximal variation in resting activity patterns as preferred-stimulus and not-preferred-stimulus is one of several possible interpretations. For example, van Loon and colleagues (van Loon et al. 2018) studied multivoxel patterns in a region of posterior fusiform cortex that was activated during visual search tasks. Subjects searched through two successive displays, where the target object for the search through each display was different. When subjects searched through the first display, the target objects for both the first and second displays could be decoded. However, the pattern that drove decoding of the second target object was the negative of the pattern that drove decoding of the same object when it served as the first target object. The authors concluded that positive and negative poles of the spatial

pattern axis corresponded to current vs prospective working memory representations. Therefore, opposing spatial activity patterns may reflect a variety of functional codes.

***Exemplars vs. prototypes***

The results showing that resting activity patterns in an ROI were related to stimulus-evoked patterns for preferred categories of the ROI raises the question of whether this relationship was based on the patterns evoked by exemplars of the category or the pattern evoked by a category mean or prototype (Posner and Keele 1968; Nosofsky 1986; Logan 2002). Previous work in anaesthetized cats (Kenet et al. 2003) and monkeys (Omer et al. 2018), for example, has shown that spontaneous activity in V1 cycles through different orientation values over time.

If the resting activity on a frame reflected a particular exemplar of a category, with the exemplar changing over frames, rather than reflecting a category mean or prototype, then the distribution over resting frames of resting-frame:template spatial correlation coefficients should be more spread for templates formed from single exemplars than from an average of different exemplars. However, we found the reverse result, with larger differences between U90 values for ‘preferred’ and ‘non-preferred’ templates formed by averaging across stimulus presentations rather than from single presentations. Moreover, U90 values were higher for categories in which single-stimulus templates were more spatially correlated (**Fig. S2**). Finally, U90 values showed at best small differences (**Fig. 8b**) for templates formed by averaging a single presentation of

four different exemplars of a category (e.g. four different faces, each presented once) or four presentations of the same exemplar (e.g. four presentations of a single face).

The issue remains open, however, partly because of power concerns (i.e. signal/noise was higher for category than exemplar templates and the heterogeneous vs. homogenous comparison was limited to 4 presentations) as well as the limited temporal resolution of fMRI, which may have obscured rapid transitions between templates in the resting state. In addition, the brain regions comprising the joint-ROIs for each category did not extend into anterior temporal cortex, likely because subjects performed a low-level detection task rather than one with a large memory component. Prior work has shown that anterior temporal regions may be particularly sensitive to individual identity (Kriegeskorte et al. 2007; Nestor et al. 2011).

***Implications for resting functional connectivity***

Previous work in humans relating resting activity to the stimulus tunings of ROIs in visual cortex has shown that functional connectivity (FC) is greater between regions with similar tunings. Studies in early visual cortex have shown that resting FC is partly governed by variables related to retinotopy (Heinzle et al. 2011; Raemaekers et al. 2014; Arcaro et al. 2015), although more variance can be explained by the FC of naturalistic stimuli, as in a movie (Wilf et al. 2017). Similarly, face-preferential regions show significant resting FC (Zhu et al. 2011; Nir et al. 2006; Zhang et al. 2009), where FC is indexed by the temporal correlation of voxel-averaged BOLD magnitudes in pairs of regions. An issue for future work concerns the resting FC organization of regions based

on the temporal correlation of spatial activity patterns rather than voxel- or vertice-averaged magnitudes (Chen et al. 2018). The overall consistency of resting-state fcMRI across subjects has inspired several attempts to specify a normative resting-state structure. Papers using different techniques have converged on a structure that is largely consistent with the structure observed in meta-analyses of task activation data, although there is certainly individual variation in this structure(Smith et al. 2009; Power *et al.* 2011; Yeo et al. 2011; Laumann et al. 2015; Cole et al. 2016; Gordon et al. 2017; Gratton et al. 2018).

The above normative structure was derived using signals whose putative representational content was not well specified since they either corresponded to single voxels or were summed over the voxels in a region. For example, the increased FC between face-preferential regions was not measured using the detailed pattern of activation within those regions. An interesting possibility is that resting state organization depends on the representational properties of the signals that are correlated across regions, where these representational properties are assessed by activity patterns. Rather than a single resting-state organization, there may be multiple FC organizations that reflect different kinds of signals (Raemaekers et al. 2014).

The current paper did not report correlations over time. However, the U90 value in a joint-ROI reflected a brain state that was spatially coherent across its constituent ROIs. This result suggests that a resting organization of brain areas can be defined from FC analyses of spatial activity patterns (Chen et al. 2018). However, the positive relationship between activation magnitude and U90 values will likely limit the extent to which this organization differs from seed-based organizations. Because regions that

tend to be co-activated during tasks also show higher FC at rest (Smith et al. 2009), the constituent ROIs forming a spatially coherent state at rest may be similarly identified using pattern-based and seed-based FC. Therefore, independent assessments of seed-based and pattern-based FC may yield resting-state organizations that are similar although not identical.

***Comparison with animal studies***

The present work was partially motivated by the pioneering studies of Grindvald, Arieli, and colleagues (Arieli et al. 1996; Tsodyks et al. 1999; Kenet et al. 2003), who used optical imaging in anaesthetized cats to show that activity patterns in V1 evoked by oriented gratings spatially matched patterns of spontaneous activity (Kenet et al. 2003). This work was recently extended to monkey by Omer and colleagues (Omer et al. 2018), who correlated spontaneous activity patterns with the differential activity pattern evoked by orthogonally oriented gratings, and compared the resulting distribution of correlation coefficients to a control distribution.

In anaesthetized monkeys, both distributions were centered on zero and the stimulus-evoked distribution had larger positive and negative tails. Presumably, the symmetric distribution reflected the columnar organization of orientation selectivity, since orthogonal gratings would activate disjoint columns. Therefore the differential spread of the two distributions reflected the similarity of resting and stimulus-evoked patterns. Interestingly, awake monkeys showed evoked and control distributions that completely overlapped, although the authors indicated that FC analyses demonstrated a

similar match of resting and evoked pattern but on a smaller spatial scale and faster timescale.

In the present work, the distributions of correlation coefficients used to compute U90 values were symmetric about zero and had larger tails for preferred than non-preferred stimulus categories. However, as noted earlier an interpretation in terms of similarity is not justified, and the results in anaesthetized monkey V1 and awake human visual cortex are not comparable. The underlying columnar architecture in the joint-ROIs is unknown, the evoked template in the current work was not formed from a contrast of orthogonal exemplars, and BOLD activity was not sampled at an analogous spatial or temporal scale.

***Limitations***

Stimuli were not controlled for low-level variables that might have differentially activated visual regions. As noted, grid-scrambled stimuli may have included contour terminators to a greater extent than single-object stimuli, increasing the activation of early visual cortex. However, this supposition is only speculative since this factor was not explicitly controlled or manipulated.

Also, although modal categories involved four presentations of 24 category exemplars, non-modal categories involved a single presentation of 96 exemplars. However, the main conclusions of the paper were clearly not due to this factor. First, greater U90 values were found not only for modal than non-modal categories, but also for non-modal than modal categories depending on the ROI. Second, significant

differences in U90 values were observed between different modal categories, which all had the same presentation schedule, and these differences were again determined by the relative activation strengths of the modal categories. For example, in the scene joint-ROI, U90 values were significantly higher for the scene category than for all single-object modal categories. Similarly, in the face and body joint-ROIs, U90 values were significantly higher for the target category than for non-animate modal categories.

Finally, the naturalistic stimuli of the present study were presented in a decidedly non-naturalistic context. Wilf et al. (Wilf et al. 2017) have shown that in early visual cortex, resting FC patterns are better accounted for by movies than by standard retinotopic stimuli, while Strappini et al. (Strappini et al. 2018) have shown that in higher-level visual cortex, resting FC patterns are better accounted for by movies than by static pictures of objects similar to those used here. Therefore, the present results may underestimate the spatial correspondences between resting and evoked activity patterns.

## Acknowledgements

This work was supported by the National Institutes of Health RO1 MH096482 to MC.

## References

Albert NB, Robertson EM, Miall RC. 2009. The resting human brain and motor learning. Curr Biol. 19:1023-1027.

Arcaro MJ, Honey CJ, Mruczek RE, Kastner S, Hasson U. 2015. Widespread correlation patterns of fMRI signal across visual cortex reflect eccentricity organization. eLife. 4.

Arieli A, Sterkin A, Grinvald A, Aertsen A. 1996. Dynamics of ongoing activity: explanation of the large variability in evoked cortical responses. Science. 273:1868-1871.

Baldassarre A, Lewis CM, Committeri G, Snyder AZ, Romani GL, Corbetta M. 2012. Individual variability in functional connectivity predicts performance of a perceptual task. Proc Natl Acad Sci U S A. 109:3516-3521.

Benson NC, Butt OH, Datta R, Radoeva PD, Brainard DH, Aguirre GK. 2012. The retinotopic organization of striate cortex is well predicted by surface topology. Curr Biol. 22:2081-2085.

Binder JR, Medler DA, Westbury CF, Liebenthal E, Buchanan L. 2006. Tuning of the human left fusiform gyrus to sublexical orthographic structure. Neuroimage. 33:739-748.

Biswal B, Yetkin FZ, Haughton VM, Hyde JS. 1995. Functional connectivity in the motor cortex of resting human brain using echo-planar MRI. Magnetic resonance in medicine. 34:537-541.

Bracci S, Op de Beeck H. 2016. Dissociations and Associations between Shape and Category Representations in the Two Visual Pathways. J Neurosci. 36:432-444.

Brainard DH. 1997. The Psychophysics Toolbox. Spatial vision. 10(4):433-6.

Chao LL, Haxby JV, Martin A. 1999. Attribute-based neural substrates in temporal cortex for perceiving and knowing about objects. Nat Neurosci. 2:913-919.

Chen RH, Ito T, Kulkarni KR, Cole MW. 2018. The Human Brain Traverses a Common Activation-Pattern State Space Across Task and Rest. Brain Connect.

Chialvo D. 2010. Emergent complex neural dynamics. Nature Physics. 6:744–750.

Cohen L, Dehaene S, Naccache L, Lehericy S, Dehaene-Lambertz G, Henaff MA, Michel F. 2000. The visual word form area: spatial and temporal characterization of an initial stage

of reading in normal subjects and posterior split-brain patients. Brain. 123 ( Pt 2):291-307.

Cole MW, Bassett DS, Power JD, Braver TS, Petersen SE. 2014. Intrinsic and task-evoked network architectures of the human brain. Neuron. 83:238-251.

Cole MW, Ito T, Bassett DS, Schultz DH. 2016. Activity flow over resting-state networks shapes cognitive task activations. Nat Neurosci. 19:1718-1726.

Dale AM. 1999. Optimal experimental design for event-related fMRI. Hum Brain Mapp. 8:109-114.

de Pasquale F, Della Penna S, Snyder AZ, Lewis C, Mantini D, Marzetti L, Belardinelli P, Ciancetta L, Pizzella V, Romani GL, Corbetta M. 2010. Temporal dynamics of spontaneous MEG activity in brain networks. Proc Natl Acad Sci U S A. 107:6040-6045.

Deco G, Jirsa VK. 2012. Ongoing cortical activity at rest: criticality, multistability, and ghost attractors. J Neurosci. 32:3366-3375.

Dehaene S, Jobert A, Naccache L, Ciuciu P, Poline JB, Le Bihan D, Cohen L. 2004. Letter binding and invariant recognition of masked words: behavioral and neuroimaging evidence. Psychological science. 15:307-313.

Downing PE, Chan AW, Peelen MV, Dodds CM, Kanwisher N. 2006. Domain specificity in visual cortex. Cereb Cortex. 16:1453-1461.

Fischl B, Sereno MI, Tootell RB, Dale AM. 1999. High-resolution intersubject averaging and a coordinate system for the cortical surface. Hum Brain Mapp. 8:272-284.

Fiser J, Berkes P, Orban G, Lengyel M. 2010. Statistically optimal perception and learning: from behavior to neural representations. Trends Cogn Sci. 14:119-130.

Fiser J, Chiu C, Weliky M. 2004. Small modulation of ongoing cortical dynamics by sensory input during natural vision. Nature. 431:573-578.

Fox MD, Corbetta M, Snyder AZ, Vincent JL, Raichle ME. 2006. Spontaneous neuronal activity distinguishes human dorsal and ventral attention systems. Proc Natl Acad Sci U S A. 103:10046-10051.

Fox MD, Snyder AZ, Vincent JL, Corbetta M, Van Essen DC, Raichle ME. 2005. The human brain is intrinsically organized into dynamic, anticorrelated functional networks. Proc Natl Acad Sci U S A. 102:9673-9678.

Fox MD, Snyder AZ, Vincent JL, Raichle ME. 2007. Intrinsic fluctuations within cortical systems account for intertrial variability in human behavior. Neuron. 56:171-184.

Gao LL, Wu T. 2016. The study of brain functional connectivity in Parkinson's disease. Translational neurodegeneration. 5:18.

Glasser MF, Sotiropoulos SN, Wilson JA, Coalson TS, Fischl B, Andersson JL, Xu J, Jbabdi S, Webster M, Polimeni JR, Van Essen DC, Jenkinson M. 2013. The minimal preprocessing pipelines for the Human Connectome Project. Neuroimage. 80:105-124.

Gordon EM, Laumann TO, Gilmore AW, Newbold DJ, Greene DJ, Berg JJ, Ortega M, Hoyt-Drazen C, Gratton C, Sun H, et al. 2017. Precision Functional Mapping of Individual Human Brains. Neuron. 95:791-807.e797.

Gratton C, Laumann TO, Nielsen AN, Greene DJ, Gordon EM, Gilmore AW, Nelson SM, Coalson RS, Snyder AZ, Schlaggar BL, et al. 2018. Functional Brain Networks Are Dominated by Stable Group and Individual Factors, Not Cognitive or Daily Variation. Neuron. 98:439-452.e435.

Greenberg AS, Esterman M, Wilson D, Serences JT, Yantis S. 2010. Control of spatial and feature-based attention in frontoparietal cortex. J Neurosci. 30:14330-14339.

Greicius MD, Krasnow B, Reiss AL, Menon V. 2003. Functional connectivity in the resting brain: a nework analysis of the default mode hypothesis. Proc Natl Acad Sci U S A. 100:253-258.

Harmelech T, Malach R. 2013. Neurocognitive biases and the patterns of spontaneous correlations in the human cortex. Trends Cogn Sci. 17:606-615.

Hasson U, Nusbaum HC, Small SL. 2009. Task-dependent organization of brain regions active during rest. Proc Natl Acad Sci U S A. 106:10841-10846.

Haxby JV, Gobbini MI, Furey ML, Ishai A, Schouten JL, Pietrini P. 2001. Distributed and overlapping representations of faces and objects in ventral temporal cortex. Science. 293:2425-2430.

Haynes JD, Rees G. 2005. Predicting the orientation of invisible stimuli from activity in human primary visual cortex. Nature neuroscience. 8:686-691.

He BJ, Snyder AZ, Vincent JL, Epstein A, Shulman GL, Corbetta M. 2007. Breakdown of functional connectivity in frontoparietal networks underlies behavioral deficits in spatial neglect. Neuron. 53:905-918.

He BJ, Snyder AZ, Zempel JM, Smyth MD, Raichle ME. 2008. Electrophysiological correlates of the brain's intrinsic large-scale functional architecture. Proc Natl Acad Sci U S A. 105:16039-16044.

Heinzle J, Kahnt T, Haynes JD. 2011. Topographically specific functional connectivity between visual field maps in the human brain. Neuroimage. 56:1426-1436.

Honey CJ, Sporns O, Cammoun L, Gigandet X, Thiran JP, Meuli R, Hagmann P. 2009. Predicting human resting-state functional connectivity from structural connectivity. Proc Natl Acad Sci U S A. 106:2035-2040.

Ingram JN, Kording KP, Howard IS, Wolpert DM. 2008. The statistics of natural hand movements. Exp Brain Res. 188:223-236.

Kamitani Y, Tong F. 2005. Decoding the visual and subjective contents of the human brain. Nature neuroscience. 8:679-685.

Kenet T, Bibitchkov D, Tsodyks M, Grinvald A, Arieli A. 2003. Spontaneously emerging cortical representations of visual attributes. Nature. 425(6961):954-956.

Kim D, Kay K, Shulman GL, Corbetta M. 2018. A New Modular Brain Organization of the BOLD Signal during Natural Vision. Cereb Cortex. 28(9):3065-3081.

Kriegeskorte N, Formisano E, Sorger B, Goebel R. 2007. Individual faces elicit distinct response patterns in human anterior temporal cortex. Proc Natl Acad Sci U S A. 104:20600-20605.

Kriegeskorte N, Goebel R, Bandettini P. 2006. Information-based functional brain mapping. Proc Natl Acad Sci U S A. 103:3863-3868.

Kriegeskorte N, Mur M, Ruff DA, Kiani R, Bodurka J, Esteky H, Tanaka K, Bandettini PA. 2008. Matching categorical object representations in inferior temporal cortex of man and monkey. Neuron. 60:1126-1141.

Kuhl BA, Chun MM. 2014. Successful remembering elicits event-specific activity patterns in lateral parietal cortex. J Neurosci. 34:8051-8060.

Laumann TO, Gordon EM, Adeyemo B, Snyder AZ, Joo SJ, Chen MY, Gilmore AW, McDermott KB, Nelson SM, Dosenbach NU, Schlaggar BL, Mumford JA, Poldrack RA, Petersen SE. 2015. Functional System and Areal Organization of a Highly Sampled Individual Human Brain. Neuron. 87:657-670.

Leo A, Handjaras G, Bianchi M, Marino H, Gabiccini M, Guidi A, Scilingo EP, Pietrini P, Bicchi A, Santello M, Ricciardi E. 2016. A synergy-based hand control is encoded in human motor cortical areas. eLife. 5.

Lewis CM, Baldassarre A, Committeri G, Romani GL, Corbetta M. 2009. Learning sculpts the spontaneous activity of the resting human brain. Proc Natl Acad Sci U S A. 106:17558-17563.

Logan GD. 2002. An instance theory of attention and memory. Psychol Rev. 109:376-400.

Martin A, Wiggs CL, Ungerleider LG, Haxby JV. 1996. Neural correlates of category-specific knowledge. Nature. 379:649-652.

Mumford D. 1992. On the computational architecture of the neocortex. II. The role of cortico-cortical loops. Biological cybernetics. 66:241-251.

Nestor A, Plaut DC, Behrmann M. 2011. Unraveling the distributed neural code of facial identity through spatiotemporal pattern analysis. Proc Natl Acad Sci U S A. 108:9998-10003.

Nir Y, Hasson U, Levy I, Yeshurun Y, Malach R. 2006. Widespread functional connectivity and fMRI fluctuations in human visual cortex in the absence of visual stimulation. Neuroimage. 30:1313-1324.

Nosofsky RM. 1986. Attention, similarity, and the identification-categorization relationship. Journal of experimental psychology General. 115:39-61.

Olshausen BA, Field DJ. 1996. Emergence of simple-cell receptive field properties by learning a sparse code for natural images. Nature. 381:607-609.

Omer DB, Fekete T, Ulchin Y, Hildesheim R, Grinvald A. 2018. Dynamic Patterns of Spontaneous Ongoing Activity in the Visual Cortex of Anesthetized and Awake Monkeys are Different. Cereb Cortex.

Oosterhof NN, Tipper SP, Downing PE. 2012. Viewpoint (in)dependence of action representations: an MVPA study. J Cogn Neurosci. 24:975-989.

Osher DE, Saxe RR, Koldewyn K, Gabrieli JD, Kanwisher N, Saygin ZM. 2016. Structural Connectivity Fingerprints Predict Cortical Selectivity for Multiple Visual Categories across Cortex. Cereb Cortex. 26:1668-1683.

Posner MI, Keele SW. 1968. On the genesis of abstract ideas. Journal of Experimental Psychology. 77:353-363.

Power JD, Cohen AL, Nelson SM, Wig GS, Barnes KA, Church JA, Vogel AC, Laumann TO, Miezin FM, Schlaggar BL, Petersen SE. 2011. Functional network organization of the human brain. Neuron. 72:665-678.

Raemaekers M, Schellekens W, van Wezel RJ, Petridou N, Kristo G, Ramsey NF. 2014. Patterns of resting state connectivity in human primary visual cortical areas: A 7T fMRI study. Neuroimage. 84:911-921.

Santello M, Baud-Bovy G, Jorntell H. 2013. Neural bases of hand synergies. Front Comput Neurosci. 7:23.

Santello M, Flanders M, Soechting JF. 1998. Postural hand synergies for tool use. J Neurosci. 18:10105-10115.

Saygin ZM, Osher DE, Koldewyn K, Reynolds G, Gabrieli JD, Saxe RR. 2011. Anatomical connectivity patterns predict face selectivity in the fusiform gyrus. Nature neuroscience. 15:321-327.

Schieber MH, Santello M. 2004. Hand function: peripheral and central constraints on performance. J Appl Physiol (1985). 96(6):2293-2300.

Serences JT, Boynton GM. 2007. Feature-based attentional modulations in the absence of direct visual stimulation. Neuron. 55:301-312.

Sha L, Haxby JV, Abdi H, Guntupalli JS, Oosterhof NN, Halchenko YO, Connolly AC. 2015. The animacy continuum in the human ventral vision pathway. J Cogn Neurosci. 27:665-678.

Shadlen MN, Newsome WT. 1994. Noise, neural codes and cortical organization. Curr Opin Neurobiol. 4:569-579.

Sharp DJ, Scott G, Leech R. 2014. Network dysfunction after traumatic brain injury. Nature reviews Neurology. 10:156-166.

Sheline YI, Raichle ME. 2013. Resting state functional connectivity in preclinical Alzheimer's disease. Biol Psychiatry. 74:340-347.

Siegel JS, Ramsey LE, Snyder AZ, Metcalf NV, Chacko RV, Weinberger K, Baldassarre A, Hacker CD, Shulman GL, Corbetta M. 2016. Disruptions of network connectivity predict impairment in multiple behavioral domains after stroke. Proc Natl Acad Sci U S A.

Smith SM, Fox PT, Miller KL, Glahn DC, Fox PM, Mackay CE, Filippini N, Watkins KE, Toro R, Laird AR, Beckmann CF. 2009. Correspondence of the brain's functional architecture during activation and rest. Proc Natl Acad Sci U S A. 106:13040-13045.

Strappini F, Wilf M, Karp O, Goldberg H, Harel M, Furman-Haran E, Golan T, Malach R. 2018. Resting-State Activity in High-Order Visual Areas as a Window into Natural Human Brain Activations. Cereb Cortex.

Tagliazucchi E, Balenzuela P, Fraiman D, Chialvo DR. 2012. Criticality in large-scale brain FMRI dynamics unveiled by a novel point process analysis. Frontiers in physiology. 3:15.

Tambini A, Ketz N, Davachi L. 2010. Enhanced brain correlations during rest are related to memory for recent experiences. Neuron. 65:280-290.

Tavor I, Parker Jones O, Mars RB, Smith SM, Behrens TE, Jbabdi S. 2016. Task-free MRI predicts individual differences in brain activity during task performance. Science. 352:216-220.

Tsodyks M, Kenet T, Grinvald A, Arieli A. 1999. Linking spontaneous activity of single cortical neurons and the underlying functional architecture. Science. 286:1943-1946.

Van Essen DC, Drury HA, Dickson J, Harwell J, Hanlon D, Anderson CH. 2001. An integrated software suite for surface-based analyses of cerebral cortex. J Am Med Inform Assoc. 8(5):443-59.

van Loon AM, Olmos-Solis K, Fahrenfort JJ, Olivers CN. 2018. Current and future goals are represented in opposite patterns in object-selective cortex. eLife. 7.

Vinckier F, Dehaene S, Jobert A, Dubus JP, Sigman M, Cohen L. 2007. Hierarchical coding of letter strings in the ventral stream: dissecting the inner organization of the visual word-form system. Neuron. 55:143-156.

Watson DM, Hymers M, Hartley T, Andrews TJ. 2016. Patterns of neural response in scene-selective regions of the human brain are affected by low-level manipulations of spatial frequency. Neuroimage. 124:107-117.

Wilf M, Strappini F, Golan T, Hahamy A, Harel M, Malach R. 2017. Spontaneously Emerging Patterns in Human Visual Cortex Reflect Responses to Naturalistic Sensory Stimuli. Cereb Cortex. 27:750-763.

Wurm MF, Ariani G, Greenlee MW, Lingnau A. 2016. Decoding Concrete and Abstract Action Representations During Explicit and Implicit Conceptual Processing. Cereb Cortex. 26:3390-3401.

Yeo BT, Krienen FM, Sepulcre J, Sabuncu MR, Lashkari D, Hollinshead M, Roffman JL, Smoller JW, Zollei L, Polimeni JR, Fischl B, Liu H, Buckner RL. 2011. The organization of the human cerebral cortex estimated by intrinsic functional connectivity. J Neurophysiol. 106:1125-1165.

Zhang H, Tian J, Liu J, Li J, Lee K. 2009. Intrinsically organized network for face perception during the resting state. Neuroscience letters. 454:1-5.

Zhu Q, Zhang J, Luo YL, Dilks DD, Liu J. 2011. Resting-State Neural Activity across Face-Selective Cortical Regions Is Behaviorally Relevant. J Neurosci. 31:10323-10330.